

Article

Screening of Raw and Modified Biochars from Food Processing Wastes for the Removal of Phosphates, Nitrates, and Ammonia from Water

Styliani E. Biliani ¹ , John Vakros ^{2,*} and Ioannis D. Manariotis ^{1,*} 

¹ Environmental Engineering Laboratory, Department of Civil Engineering, University of Patras, 26504 Patras, Greece

² School of Sciences and Engineering, University of Nicosia, 2417 Nicosia, Cyprus

* Correspondence: vakros@chemistry.upatras.gr (J.V.); idman@upatras.gr (I.D.M.)

Abstract: The aim of this work was to compare the performance of biochar from various food processing wastes of different origin for the removal of different nutrients from water. Eggshells (EGS), rice husk (RH), and coffee biochars were pyrolyzed at 400 and 800 °C and were examined for the removal of phosphates, nitrates, and ammonia nitrogen. The raw materials were also modified with magnesium chloride in order to investigate their sorption behavior. The highest sorption capacity (q_{\max}) for phosphates and ammonium was observed with EGS pyrolyzed at 800 °C and was 11.45 mg $\text{PO}_4^{3-}\text{-P/g}$ and 11.59 mg $\text{NH}_3\text{-N/g}$, while the highest nitrates sorption capacity was observed with the magnesium-modified RH pyrolyzed at 800 °C (5.24 mg $\text{NO}_3^-\text{-N}$). The modified EGS biochars pyrolyzed at 800 °C had almost the half the sorption capacity for phosphates and nitrates compared to the unmodified materials. The modification of RH pyrolyzed at 800 °C resulted in higher sorption capacity by 34 and 158% for phosphates and ammonium, respectively. The coffee raw and modified biochars were less efficient in nutrient removal compared to the other materials. The specific surface area values of the biochars examined is not a decisive factor for nutrient sorption. The reaction between magnesium and calcium (for the eggshell samples) ions with phosphates is responsible for the higher sorption efficiency. On the other hand, the presence of magnesium and calcium ions has a detrimental effect on the sorption of $\text{NH}_3\text{-N}$.

Keywords: food processing wastes; biochar; magnesium modification; nutrient removal; kinetics



check for updates

Citation: Biliani, S.E.; Vakros, J.; Manariotis, I.D. Screening of Raw and Modified Biochars from Food Processing Wastes for the Removal of Phosphates, Nitrates, and Ammonia from Water. *Sustainability* **2022**, *14*, 16483. <https://doi.org/10.3390/su142416483>

Academic Editor: Agostina Chiavola

Received: 3 November 2022

Accepted: 6 December 2022

Published: 9 December 2022

Publisher's Note: MDPI stays neutral with regard to jurisdictional claims in published maps and institutional affiliations.



Copyright: © 2022 by the authors. Licensee MDPI, Basel, Switzerland. This article is an open access article distributed under the terms and conditions of the Creative Commons Attribution (CC BY) license (<https://creativecommons.org/licenses/by/4.0/>).

1. Introduction

Wastewater and drainage waters that outflow in water bodies contain nutrients that increase eutrophication [1,2]. Controlling nutrient outflow can also lead to eutrophication reduction. The removal of nutrients from water can be achieved by various methods either by physicochemical or biological processes [3]. The sorption capacity of sorbents on nutrient removal depends on the material type, origin, and treatment [4]. Therefore, the choice of the optimal methodology for nutrient removal should be chosen considering the above factors. The cost of sorbent production is also one significant parameter for the sustainability of the process. Sorption processes have been examined during the last years in order to remove nutrients from water using natural zeolite, calcite, sand and iron products [5], and biochar or modified biochar [6,7].

Biochar (BC) is a porous carbon material usually derived from lignocellulosic biowaste or from other mixed food wastes such as bones, eggshell, etc., through the thermal process with interesting adsorption properties [8]. Although biochar fully consists of carbon content and ash, its physicochemical characteristics are greatly influenced from the type of biomass used and the carbonization conditions [9]. The carbonization process usually is one thermochemical conversion method such as pyrolysis, hydrothermal carbonization,

gasification, and torrefaction [10,11]. Therefore, the properties of biochar and its efficiency in different processes depend on the preparation conditions and the raw biomass.

Feedstock of different origins have been investigated in order to reduce nutrients with an environmentally friendly method. The emphasis has been provided to the availability and use of low-cost materials, individually or by mixing various feedstocks [12]. The beneficial use of wastes from the food industry, as sorbent materials, can contribute to the reduction in disposed wastes. After sorption, the rich in nutrient sorbent materials can be used as slow-release fertilizers [13,14] or even for soil improvement [15,16].

Coffee is one of the most consumed beverages all over the world. In 2016, the production of coffee reached about 9×10^6 tonnes [17]. The carbon and oxygen in spent coffee grounds comprise almost 84% and 12% in an atomic ratio [18]. The main content of the macronutrients of spent coffee grounds in g/kg of dry matter (DM) is 500.34 carbon, 1.77 calcium, 25.61 nitrogen, 1.53 phosphorus, 1.48 magnesium, 5.06 potassium, 0.13 sodium, and 0.87 sulphur [19]. Coffee spent grounds are used as organic mineral fertilizers or soil conditioner [19]. Rice husk (RH) represents at least 20% of the rough rice weight, which yields about 1.5×10^{11} kg/year, placing it among the most abundant agricultural product worldwide. Rice cultivation is a significant crop in Greece, given that it is the third largest producer of rice in the European Union (EU) [20]. RH is a lignocellulosic material that consists of from 28.6 to 43.3% cellulose, from 22.0 to 29.7% hemicellulose, from 19.2 to 24.4% lignin, and from 17 to 20% ash [21]. RH is used for practical purposes such as for production of biofuels, energy, and fertilizers [22]. Eggshell wastes have been ranked as the 15th worst food industry pollution problem by the Environmental Protection Agency. They are considered as a major source of environmental pollution when not properly disposed of in specified locations. The global eggshell quantity for 2018 was 8.58×10^6 tonnes [23]. Chicken eggshells consist of from 47.63 to 51.7% carbohydrates, from 3.0 to 4.38% crude fiber, 0.37% lipid, from 1.35 to 1.40% crude protein, and from 43.5 to 45.29% ash [24]. The main content of macronutrients of chicken eggshells is in g/kg DM 145.43 carbon, 231.67 calcium, 8.47 nitrogen, 1.00 phosphorus, 2.44 magnesium, 0.66 potassium, 0.74 sodium, and 0.78 sulphur [19].

Eggshells can be used in many aspects such as soil conditioner, food additive, calcium supplement, agricultural fertilizers, and sorbent [19,24]. The biochar from eggshells has been used for the removal of organic pollutants [25] and phosphorous [26,27]; it has achieved over 90% removal of phosphorus.

The modification of feedstock materials using $MgCl_2$ [28,29], and $FeCl_3$ [29] has been used for the enhancement of the removal of phosphates and/or nitrates from water. The increased surface area and the porous structure of MgO-biochar nano flakes were decisive factors for the removal of anions due to the increase in adsorption sites [28]. The modification of sawdust and sediment biochar by $FeCl_3$ and $MgCl_2$ resulted in phosphorus recovery of from 61.2 to 100% and from 53.1 to 100%, respectively [29]. The authors reported that the pristine biochar did not show any removal capacity for phosphates. The importance of magnesium modification was also reported for the modification of oak wood and paprika waste for phosphate uptake, which enhanced the phosphorous uptake from relatively low levels of from 66.4 to 70.3%, compared to from 2.1 to 3.6% of the pristine biochar [30].

Although considerable research has been conducted on nutrient removal using biochar, the behavior of pristine biochar pyrolyzed at different temperatures and their modification for the removal of different nutrients needs further investigation. The aim of our study was to investigate the effectiveness of biochar produced from easily available food processing wastes, the effect of pyrolysis temperature, and the modification of biochar for the removal of nutrients from water. The use of food processing wastes as a biochar material is an ecological product that reduces wastes and strengthens the circular economy. Easily available biomass from chicken eggshells, spent coffee grounds, and rice husk were used for the production of biochar pyrolyzed at 400 and 800 °C. The modification of biochar with magnesium was also conducted to examine their performance. Ammonia nitrogen, nitrates,

and phosphates were the target nutrients and the evaluation of the biochar's sorption capacity was conducted by batch kinetic and isotherm experiments.

2. Materials and Methods

2.1. Preparation of Biochar

Different materials have been investigated in order to find the material that can adsorb different kind of nutrients with the highest efficiency level. Biochar has been investigated at three types of feedstocks eggshells, rice, and coffee. The chicken eggshells (EGS) were obtained from a local pastry factory of Entelvais S.A., Patras, Greece. The rice husk (RH) was produced from the rice processing factory of Agrino S.A., Agrinio, Greece. The spent coffee grounds were obtained after espresso coffee was brewed through coffee machines in Patras coffee shops. The eggshells were thoroughly washed with tap water and then with distilled water. All the materials were dried overnight at 60 °C and were separately weighted and placed into ceramic and/or quartz vessels that were closed with their respective caps (Figure S1). These vessels were custom-made not to allow oxygen to enter the vessels at high temperatures. The vessels with each material were placed in a gradient temperature furnace (LH 60/12, Nabertherm GmbH, Lilienthal/Bremen, Germany) at temperatures of 400 and 800 °C. The mass of each material was weighted before and after the pyrolysis process and the weight loss due to pyrolysis was calculated.

The sorption efficiencies of each raw material (eggshells, spent coffee grounds, and rice husks) were also examined after modification with MgCl₂·6H₂O [31]. Briefly, the raw material was impregnated in 3 M MgCl₂·6H₂O for 18 h. The material was removed and washed with distilled water. The material was dried in an oven and pyrolyzed at 400 and 800 °C. The biochars, hereafter, are denoted as "Material name" "Pyrolysis temperature", while in the magnesium modified materials the term "Mg" is added. For example, EGS400 and EGS400Mg stand for eggshells pyrolyzed at 400 °C and magnesium-modified eggshells pyrolyzed at 400 °C, respectively.

2.2. Sorption Experiments

2.2.1. Kinetic Experiment

The individual nutrient solutions of 10 mg PO₄³⁻-P/L, 7.77 mg NH₃-N/L and 2.26 mg NO₃⁻-N/L were prepared in order to examine the removal of nutrients at higher phosphorus concentrations compared to nitrogen compounds. A volume of 40 mL of each nutrient solution was transferred into a 40 mL polypropylene test tube containing 10 mg of biochar. The tubes were hooked on a rotator (J.P. Selecta s.a., Barcelona, Spain) for a specified time (12, 24, 48, 72, 96, and 168 h). Subsequently, the tubes were placed vertically for the biochar to settle and the liquid was filtered via a 0.22 µm syringe filter.

2.2.2. Isotherm Experiment

The equilibrium time for the majority of our materials was 48 h according to the kinetic analysis results. Only the materials with the higher sorption capacity (EGS800, EGS800Mg, RH800, and RH800Mg) were examined at different concentrations of 0, 2.5, 5, 10, and 20 mg PO₄³⁻-P/L, 0, 2, 4, 8, and 16 mg NH₃-N/L and 0, 2, 4, 8, and 16 mg NO₃⁻-N/L.

2.3. Sorption Models

2.3.1. Kinetic Model

The nutrient removal was simulated with various kinetic models. The first-order kinetic model is written:

$$\frac{dq}{dt} = -k_1 q_t \quad (1)$$

where q (mg/g) is the quantity of nutrient sorbed per unit mass of biochar at a given time t , k_1 (h⁻¹) is the first-order rate constant, and t (h) is the contact time. By integrating Equation (1), we obtain the linear form:

$$\ln q_t = \ln q_e - k_1 t \quad (2)$$

where q_e (mg/g) is the quantity of nutrient sorbed per unit mass of biochar at the equilibrium. The pseudo first-order model is:

$$\frac{dq}{dt} = -k_{1p}(q_e - q) \quad (3)$$

where k_{1p} (h^{-1}) is the pseudo first-order rate constant. The linear form of Equation (3) is:

$$\ln(q_e - q_t) = \ln q_e - k_{1p}t \quad (4)$$

The second-order model is:

$$q = \frac{q_e}{1 + q_e k_2 t} \quad (5)$$

where k_2 (g/mg·h) is the second-order rate constant. The linear form of Equation (5) is:

$$\frac{1}{q} = \frac{1}{q_e} + k_2 t \quad (6)$$

Finally, the pseudo second-order model is written:

$$\frac{dq}{dt} = k_{2p}(q_e - q_t)^2 \quad (7)$$

where k_{2p} (g/mg·h) is the of pseudo second-order rate constant. The linear form of Equation (7) is:

$$\frac{t}{q} = \frac{1}{q_e} t + \frac{1}{k_{2p} q_e^2} \quad (8)$$

To investigate the potential role of nutrient diffusion on sorption materials, the Weber–Morris model was used [32]:

$$q = k_{id} t^{1/2} + C \quad (9)$$

where k_{id} is the intra-particle diffusion rate constant ($\text{mg/g h}^{1/2}$) and C (mg/g) is the y-intercept. The linearity of the plot of q versus $t^{1/2}$ denotes the presence of intra-particle diffusion. If $C = 0$, then intra-particle diffusion is the rate-controlling step, whereas if $C \neq 0$, intraparticle diffusion is not the rate-controlling step, but film diffusion plays an important role in the nutrient sorption process.

In order to assess which process, external mass transfer, or intra-particle diffusion exerts greater influence on the rate of its nutrient sorption, the Boyd film-diffusion model was employed. This model assumes that the main resistance to diffusion is the boundary layer surrounding the particle and is expressed as [33]:

$$F(t) = 1 - \left(\frac{6}{\pi^2}\right) \sum_{m=1}^{\infty} \left(\frac{1}{m^2}\right) e^{-m^2 B t} \quad (10)$$

where $F(t)$ is the fraction of the solute sorbed at different times t :

$$F(t) = \frac{q}{q_e} \quad (11)$$

where q and q_e are the nutrient uptake (mg/g) at time t and at equilibrium, respectively, m is the number of particles and B is obtained from the following equation:

$$B = \frac{D_i \pi^2}{r^2} \quad (12)$$

where D_i is the internal diffusion coefficient and r is the radius of the sorbent particle. Reichenberg, 1952 [34], after applying Fourier transform and integration, managed to obtain the following approximations:

$$B_t = \begin{cases} -0.4977 - \ln(1 - F(t)), & F(t) > 0.85 \\ 2\pi - \frac{\pi^2 F(t)}{3} - 2\pi\sqrt{1 - \frac{\pi F(t)}{3}}, & F(t) < 0.85 \end{cases} \quad (13)$$

2.3.2. Isotherm Model

The experimental data were fitted to three isotherm models linear, Freundlich, and Langmuir. The linear isotherm model is described by the equation

$$q_e = K_H C_e \quad (14)$$

where K_H (L/g) is the Henry's constant.

The Langmuir isotherm model is:

$$\frac{C_e}{q_e} = \frac{1}{q_{max} K_L} + \frac{C_e}{q_{max}} \quad (15)$$

where C_e (mg/L) is the equilibrium concentration in the solution, q_{max} (mg/g) is the maximum monolayer sorption capacity, and K_L (L/mg) is the constant of Langmuir model.

The Freundlich model is:

$$\ln q_e = \ln K_F + N \ln C_e \quad (16)$$

where K_F ((mg/g)(L/mg)^N) is the sorption constant for the Freundlich model and N is the Freundlich exponent related to sorption nonlinearity, indicative of the distribution of the active sites on the sorbent.

The available isotherm model equations were compared based on the correlation coefficient (R^2) obtained from the corresponding linear plot and the residual sum of squares (RSS):

$$RSS = \sum_{i=1}^n (q^{exp} - q^{calc})^2 \quad (17)$$

where q^{exp} and q^{calc} are experimental and predicted by the model values of q (mg/g), respectively, n is the number of experimental values, and the subscript $i = 1$ to n indicates the appropriate sample.

2.4. Biochar Characterization

A scanning electron microscope (SEM, JEOL JSM6300) equipped with an EDS was used for the determination of morphology. The point of zero charge (pzc) was measured through a salt addition method [35]. The PZC values were determined in 0.1 M NaNO₃ (8.5 g/L) solution at 25 ± 2 °C. A mass of 0.2 g of biochar was transferred into 50 mL polypropylene tubes containing 40 mL of 0.1 M NaNO₃. The pH of the suspension was then adjusted to an initial pH value of 4, 5, 6, 7, 8, 9, 10, 11, or 12 using either 0.1 M HNO₃ or 0.1 M NaOH solutions and an Orion pH-meter model 710 A. Each tube was placed into a rotator (J.P. Selecta, s.a., Barcelona, Spain) for 24 h. The ΔpH (the difference between final and initial pH) values were then plotted against the initial pH values. The initial pH at which ΔpH is zero was extracted to be the PZC.

The specific surface area, (SSA) of each sorbent was determined with the N₂ adsorption isotherms in liquid N₂ temperature (Tristar 3000 porosimeter, Micromeritics) and using the BET method. The X-ray diffraction (XRD) patterns were recorded using a Bruker D8 Advance diffractometer. The Fourier transform infrared (FTIR) spectrum was recorded

at 4000–400 cm^{-1} using a Perkin Elmer Spectrum RX FTIR system with a KBr pellet with 1% *w/w* BC.

2.5. Analytical Methods

The phosphates were measured by the persulfate method and ascorbic colorimetric technique [36]. The nitrates were measured by the sodium salicylate method [37] and ammonium was measured by the phenate method [36]. All the determinations were conducted in duplicate and the data were showed as mean \pm SD (standard deviation). The data were analyzed and plotted by IGOR Pro (WaveMetrics, Inc., Lake Oswego, OR, USA).

3. Results and Discussion

3.1. Biochar Characterization

The feedstock composition and pyrolysis temperature affect the pzc of biochar (Table 1). The pzc values of 6.74 and 6.30 for rice husk biochar pyrolyzed at 300 and 700 °C, respectively, were also reported [38]. However, other researchers [20] mentioned that pzc at rice husk biochar pyrolyzed at 700 and 850 °C was 7.4 and 7.8, respectively. In the present study, the pyrolysis of the rice husk at 800 °C had a drastic increase in the pzc value to 10.0. The increase in the pyrolysis temperature from 300 to 600 °C caused a decrease in pzc values using solid mill wastes, oak acorn shells, and deseeded carob pods [39]. The pzc of magnesium-impregnated biochars was above eleven in the two pyrolysis temperatures tested. The modification of biomass with $\text{MgCl}_2 \cdot 6\text{H}_2\text{O}$ resulted in the increase in pzc since the positive charged magnesium attached to their surface [28].

Table 1. Pzc and surface characteristics of materials tested.

Material	Pzc	BET Surface Area (m^2/g)	Pore Volume (cm^3/g)	Pore Size (nm)	Pore Width (Å)	Yield (%)
EGS	9.0					96.9
EGS400	10.0	0.95	0.0027	11.3	113.2	92.8
EGS800	10.3	0.51	0.0066	11.7	117.3	97.7
EGS400Mg	11.4	0.56	0.0011	8.7	86.7	94.3
EGS800Mg	11.3	0.14	0.0012	0.85	8.5	
RH	7.0					44.3
RH400	6.4	0.60	0.1032	1.2	11.5	30.7
RH800	10.0	253	0.1333	2.1	21.1	54.6
RH400Mg	11.0	15.1	0.0363	9.6	96.1	33.3
RH800Mg	11.8	115	0.0645	13.1	131.2	
Coffee	6.1					34.5
Coffee400	7.5	0.32	0.0061	11.7	117.2	24.6
Coffee800	6.2	109	0.0481	1.8	17.8	41.4
Coffee400Mg	11.1	25.8	0.0879	13.6	136.4	36.9
Coffee800Mg	11.6	37.2	0.1102	11.8	118.5	96.9

The pzc is the pH where the total charge of the surface is zero. The pzc of raw eggshells was 9.0, rice husk neutral (7.0), and coffee 6.1, indicating the effect of the raw materials' compositions. The effect of the pyrolysis temperature was not the same for the three materials tested. The pyrolysis of eggshells caused higher pzc values; from 9, for the raw EGS, to about 10 for the pyrolyzed eggshells. On the other hand, the pzc of the rice husk biochar at 400 °C was lower (6.4) compared to the raw material, but increased to a value of 10.0 at 800 °C. The pzc of the coffee biochar increased from 6.1 of the raw material to 7.5 at 400 °C, but reduced to 6.2 at 800 °C, yielding a similar value as the raw material. The spent coffee grounds pyrolyzed at 850 °C had almost neutral surfaces (pzc = 6.9) [18].

The increase in pzc with the temperature can be attributed to the removal of the oxygen-containing surface species of the biochar. Indeed, these species, phenolic–OH and –COOH, usually groups have moderate acidity. With the increase in pyrolysis temperature, these species removed from the surface and, as a result, the pzc increased. One other

reason is that the minerals, usually oxides and carbonates, have basic properties and their concentrations increase with the pyrolysis temperature, since more organic phases burned in higher temperatures, increasing the surface basicity and, thus, the pzc values.

The SEM elemental analysis showed high oxygen content for modified or unmodified materials (Table 2). The low content of raw eggshells in the oxygen enhanced their sorption effectiveness [24]. The oxygen content was almost the same before and after modification with coffee having the lower content (from 36 to 37%) and the rice husks greater (from 51 to 53%). The modification of biomass with magnesium chloride resulted in the higher Mg content of biochars, which is expected to increase the sorption capacity [29,31]. In addition, the Cl content was increased in the Mg-modified biochars. The Mg content of the unmodified biochars was around from 0.1 to 0.3% and after modification increased from 4 to 37% for the three materials pyrolyzed at 400 and 800 °C. The modified EGS biochars have (i) the lower SSA values, (ii) higher crystallinity, (iii) higher pzc values, and (iv) higher content of Ca and show the lowest content in Mg, which can be attributed to these factors that cause the deposition of Mg²⁺ ions during modification of the samples to be difficult [25]. The increase in the pyrolysis temperature also increases the Mg content as can be seen in Table 2. It should be mentioned that a higher pyrolysis temperature removes the volatile species from the biochar. The chlorine content increased from 0 to 4 for the unmodified biochars and 3.5% for the eggshells, from 0 to 37 and 20% for RH BC, and 0 and 6.7% for coffee biochars after magnesium modification, respectively. The biochar modification also increased the calcium content to 79 and 148 times for the eggshells pyrolyzed either at 400 or 800 °C, respectively. Calcium was not detected in RH and coffee materials. Based on the EDX analysis, calcium was found only with RH400 (0.42%) and RH800Mg (3.38%). The magnesium modification of the ground coffee bean wastes pyrolyzed at 550 °C resulted in the reduction in the calcium content of about 3.7 times compared to the ground coffee bean [31].

Table 2. Elemental analysis of the materials tested determined by EDX analysis.

Material	Element (%)									
	C	O	Na	Mg	P	S	Si	Cl	K	Ca
EGS	48.5	50.3		0.35	0.32	0.06				0.64
EGS400	50.4	48.76		0.31						0.53
EGS800	52.21	47.2		0.33						0.26
EGS400Mg		48.8		4.16				4.44		42.6
EGS800Mg		50.1	0.23	5.14				3.35	2.68	38.50
RH		67.6					31.5		0.81	
RH400		53.14					44.64		1.8	0.42
RH800		51.8					46.2		2.0	
RH400Mg		50.08		9.89			27.03		13.0	
RH800Mg		36.84		37.13			15.91	6.74		3.38
Coffee	60.8	38.74		0.12						
Coffee400	62.6	37.13		0.12		0.15				
Coffee800	63.25	36.48		0.12		0.15				
Coffee400Mg		42.4		20				37.6		
Coffee800Mg		44.7		35.3				20.0		

The values of SSA are presented in Table 1. Generally, the values of SSA are low for the biochars prepared at 400 °C. This is in accordance with different studies [20,40] where it was found that temperatures higher than 700 °C are usually needed for increasing the SSA of the biochar. This is because in high pyrolysis temperatures the evolution of O containing species as gases creates new pores and increases the SSA. This is confirmed also in this study. The EGS biochars exhibit low SSA, as the result of high quantities of CaCO₃ were detected. Since CaCO₃ is not affected from the pyrolysis temperature, there are not any significant changes in SSA values. The addition of Mg significantly decreases the SSA values of biochars pyrolyzed at 800 °C, even for the EGS biochar. This can be attributed to

the formation of different Mg species on the surface of biochar such as MgO, MgCO₃, or even MgCl₂ and the blocking of pores created during the high pyrolysis process. The effect of adding Mg is different in the lower temperature. The modified biochars pyrolyzed at 400 °C exhibited higher values of SSA, especially in the high carbon-content samples, such as RH and coffee. This is due to the pyrolysis step after impregnation. The presence of Mg is beneficial for the transformation of raw biomass to biochar with moderate SSA values.

The FTIR spectra of the biochars studied are presented in Figure 1. As can be seen in the EGS samples, there are two intense and sharp peaks at 876 and 712 cm⁻¹. These peaks are due to CaCO₃; there are some new peaks centered about 2517 cm⁻¹ [41]. These peaks have been detected in samples of CaCO₃ with Mg quantities. Depending on the content of Mg, these peaks can be shifted to higher wavenumbers. It is the result of the partial substitution of Ca ions with Mg. The free carbonate ions exhibit four intramolecular vibrations: ν₁ (symmetrical stretching), ν₂ (bending beyond the plane), ν₃ (symmetrical stretching), and ν₄ (bending in the plane). The ν₄ can be used for the identification of carbonates minerals; CaCO₃ is centered at 712 cm⁻¹, for MgCO₃ is shifted at 748 cm⁻¹ while at a partial substitution of Ca with Mg the peak can be observed between these limits, while new peaks centered at about 2520 cm⁻¹ are due to ν₁ + ν₃ vibrations.

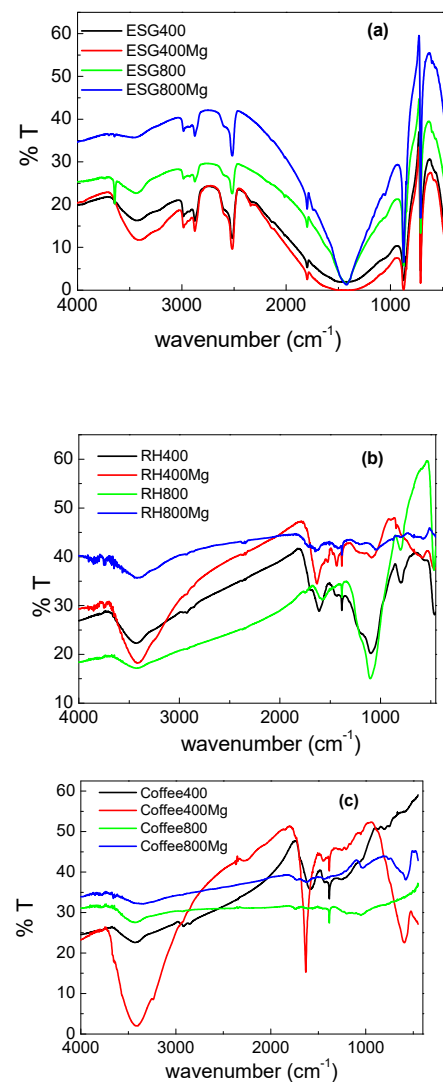


Figure 1. FTIR spectra of the biochars studied; biochars from (a) EGS, (b) RH, and (c) Coffee.

The FTIR spectra of the RH biochars are presented in Figure 1b. There is a broad peak centered at 3400 cm⁻¹ due to the –OH groups and adsorbed water molecules. This

peak is significantly lower in the biochar pyrolyzed at 800 °C. This was also observed in a previous study [20] and it is due to the higher extent of the removal of O species in 800 °C. Additionally, the peaks presented between 1600 and 1400 cm^{-1} are less intense in higher pyrolysis temperatures. Finally, no significant differences can be detected with the Mg modification.

Similar spectra were collected for the coffee biochars. Only the Coffee400Mg sample has a different spectrum. There is a sharp peak at 1632 cm^{-1} and the broad peak at 3400 cm^{-1} is very intense. The peak at 1632 cm^{-1} is probably due to C=O bonds, while the peak at 3400 cm^{-1} is due to –OH groups. Both peaks are smaller after pyrolysis at 800 °C due to the significant removal of O species, while in the biochar pyrolyzed at 400 °C the modification of the raw coffee biomass with Mg is beneficial not only in terms of SSA values but also in the presence and amount of surface O groups.

The XRD patterns of the biochars from eggshells presented in Figure 2a confirm the presence of CaCO_3 in the biochars since all the sharp peaks represent CaCO_3 . Additionally, no significant differences of Mg ions were detected with the modification. This can be explained from the low content of Mg remaining in the modified biochars. The Mg content is not enough to substitute the Ca in the CaCO_3 form in a high extent and thus is not detected during the XRD analysis. Only in the EGS800Mg is there a small shift of the main peak from $2\theta = 29.4^\circ$ to 29.6° .

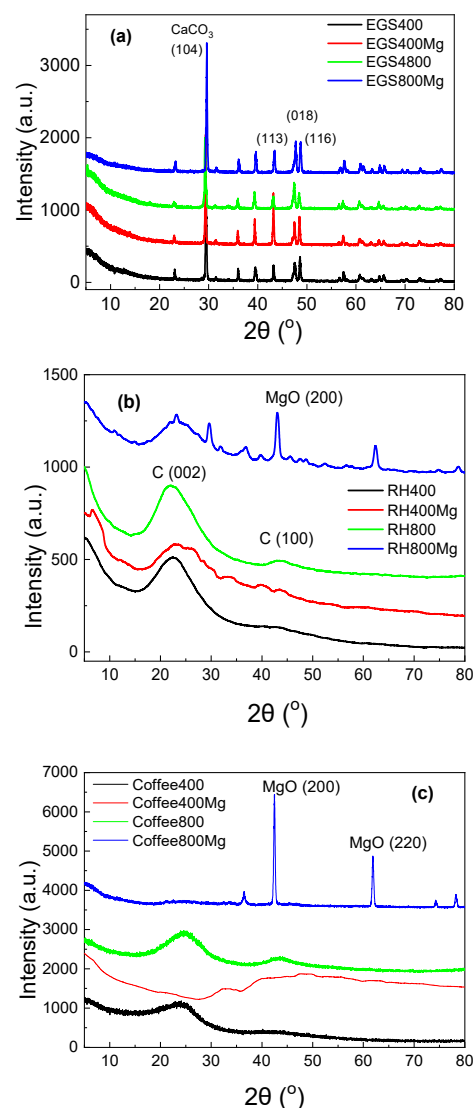


Figure 2. XRD patterns for the biochars studied; biochars from (a) EGS, (b) RH, and (c) Coffee.

The XRD patterns for the biochars prepared from rice husk have a broad peak centered at about 22° , which is typical for the amorphous graphitic phase (the peak corresponds to (002) crystal plane) followed by a smaller peak at 43° , which represents the sp^2 carbon atoms [42,43]. This peak can be seen clearly in the RH800 sample.

Finally, the unmodified coffee biochars have the same two wide peaks for the amorphous graphitic phase, while the main peaks for the Coffee800Mg sample are those corresponding to MgO formation (43° and 62°). The modified biochar in 400°C has an amorphous pattern pointing out that the low pyrolysis temperature is not enough for the formation of Mg crystal phases.

3.2. Effect of Contact Time on Sorption Process

The eggshells pyrolyzed at 400 and 800°C phosphate concentrations reached a plateau at 24 h (Figure 3a). The phosphate sorption was higher with the modified materials and was 20 and 30 mg/g at 400 and 800°C , respectively (Figure 3a), although the unmodified materials reached a plateau earlier. The increase in the pyrolysis temperature did not affect the sorption capacity of unmodified eggshells but improved the sorption capacity of magnesium-modified eggshell biochars.

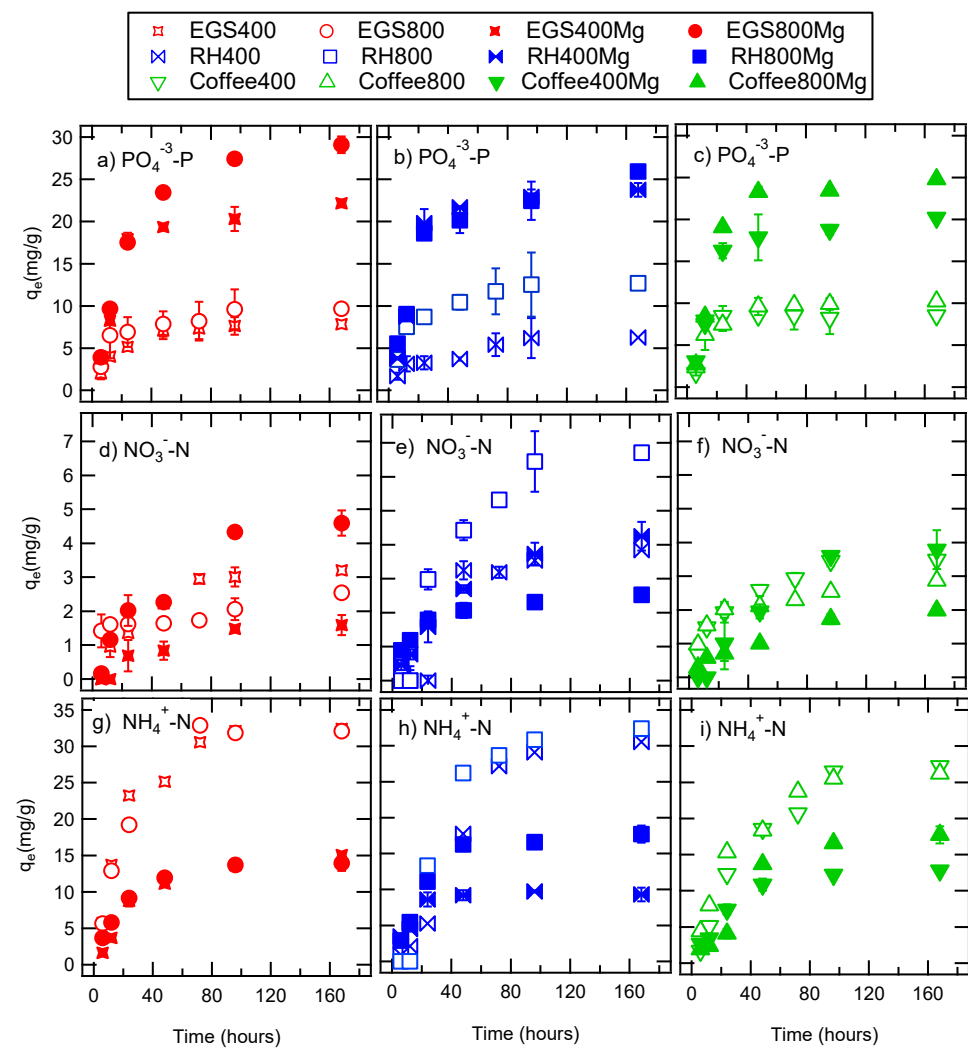


Figure 3. Effect of contact time on uptake of: phosphates at an initial concentration of $10\text{ mg PO}_4^{3-}\text{-P/L}$ for (a) EGS, (b) RH, and (c) Coffee; nitrates at an initial concentration of $2.26\text{ mg NO}_3\text{-N/L}$ for (d) EGS, (e) RH, and (f) Coffee; and ammonia at an initial concentration of $7.77\text{ mg NH}_3\text{-N/L}$ for (g) EGS, (h) RH, and (i) Coffee.

The phosphate concentrations with rice husks reached a plateau even from 24 h. The magnesium-modified materials reached an uptake of 30 mg/g at both pyrolysis temperatures (Figure 3b). Although, the pyrolysis temperature did not affect the sorption capacity of the modified biochars, while the higher pyrolysis temperature of the raw materials led to higher sorption of phosphates (Figure 3b). The increase in the pyrolysis temperature increases the surface of the biochar [44], which results in higher phosphorous removal [45]. The rice husk at 800 °C reached a plateau at 96 h, while for the other RH biochars a plateau was reached after 48 h. The coffee biochar reached a plateau with phosphates after 24 h (Figure 3c). The modification of the coffee biochar with magnesium resulted in an increase in the sorption capacity at both pyrolysis temperatures. The increase in the pyrolysis temperature improved phosphate sorption only in the case of modified biochars. The effect of the pyrolysis temperature (from 300 to 600 °C) for the production of biochar from the co-pyrolysis of fenton sludge and bamboo was also examined [46]. The maximum phosphorus sorption capacity was observed at 400 °C for the fenton sludge and was 8.77 mg/g.

The phosphate sorption capacity was 12.5 mg/g at 96 h for RH800, compared to 10 mg/g at 96 h for EGS800. Although RH800Mg reached an uptake of phosphates of 25.5 mg/g at 168 h, EGS800Mg reached a plateau quite earlier at 96 h and an uptake of 27.5 mg/g.

As seen for the eggshells pyrolyzed at 400 and 800 °C, a plateau was reached for the nitrates after about 96 h (Figure 3b). During the first 24 h, the nitrate sorption using the RH800 was practically zero (Figure 3d). On the contrary, the modified RH biochars performed better during the first 24 h, compared to the unmodified biochars. The RH800 presented higher nitrate sorption capacity compared to RH400. The coffee-based biochars reached a plateau after 24 h with nitrates (Figure 3f). The modification of the coffee biochar led to an increased sorption capacity for nitrates at both pyrolysis temperatures. The pyrolysis temperature did not affect the sorption ability of the unmodified coffee biochars for nitrates. The modification of coffee biochar at 400 °C resulted in a slightly better sorption efficiency compared to the unmodified coffee biochars, while the modification of coffee at 800 °C provided the worst results. The nitrate sorption capacity was 6.5 mg/g at 96 h for RH800, compared to 2 mg/g at 96 h for EGS800. The nitrate sorption was faster with EGS800Mg (4.5 mg/g at 96 h) compared to RH800Mg with (3 mg/g at 168 h).

The pyrolysis temperature did not affect the ammonia sorption of the unmodified biochars. Generally, modification inhibited the ammonia uptake (Figure 3g–i). A plateau was reached for ammonia nitrogen after 72 h with unmodified EGS (Figure 3g). Similarly, with nitrates, the sorption of ammonia by RH400 and RH800 was practically zero within the first 24 h (Figure 3h). As seen in Figure 3i, the unmodified EGS and RH reached similar sorption capacity after 168 h, while the unmodified coffee biochar presented a slightly lower capacity.

The experimental results were better simulated with the pseudo first- and second-order kinetic models (Table 3) and the latter better fitted the experimental data for phosphates and nitrates of all the materials tested. The pseudo second-order constant of phosphates for all materials was quite higher with unmodified materials compared to the modified. The k_2p values were 4 and 3.5 times higher for the EGS400 and EGS800, 3 and 2.5 times higher for the RH 400 and RH 800, and 13 and 3.5 times for the Coffee400 and Coffee800, compared to the corresponding modified material, respectively. Coffee400 had the higher k_2p value (0.013 g/mg·h) and the EGS400Mg and Coffee400Mg the lower (0.001 g/mg·h).

Table 3. Estimated parameters for the Kinetic models employed.

Material	Kinetic Model							
	Pseudo First-Order				Pseudo Second-Order			
	$-k_{1p}$ (h^{-1})	q_e (mg/g)	R^2	RSS	q_e (mg/g)	k_{2p} ($g/mg \cdot h$)	R^2	RSS
PO_4^{-3} -P								
EGS400	0.041	8.39	0.790	3.1	8.67	0.008	0.997	24
EGS800	0.036	6.10	0.975	0.98	10.42	0.007	0.994	50
EGS400Mg	0.030	26.64	0.979	70	35.71	0.001	0.989	16
EGS800Mg	0.024	13.78	0.773	20	25.32	0.002	0.982	15
RH400	0.040	11.26	0.944	2.3	7.18	0.006	0.969	7.4
RH800	0.040	7.60	0.825	0.58	13.81	0.005	0.998	12
RH400Mg	0.021	6.21	0.991	1.2	29.16	0.002	0.993	25
RH800Mg	0.017	16.69	0.938	21	27.62	0.002	0.974	34
Coffee400	0.036	6.51	0.926	126	9.15	0.013	0.977	76
Coffee800	0.046	1.20	0.606	2.0	11.19	0.007	0.993	14
Coffee400Mg	0.025	7.22	0.593	5.4	30.77	0.001	0.924	31
Coffee800Mg	0.012	6.01	0.704	4.1	27.62	0.002	0.974	28
NO_3^{-} -N								
EGS400	0.007	1.14	0.790	270	4.05	0.006	0.983	15
EGS800	0.033	3.74	0.968	302	2.58	0.024	0.984	5
EGS400Mg	0.030	5.71	0.928	371	5.95	0.003	0.943	10
EGS800Mg	0.030	2.15	0.956	229	2.20	0.008	0.960	28
RH400	0.034	9.56	0.939	205	4.25	0.012	0.995	1.2
RH800	0.031	5.13	0.893	149	8.60	0.003	0.988	17
RH400Mg	0.022	1.56	0.944	222	2.71	0.026	0.999	50
RH800Mg	0.022	4.49	0.982	352	6.31	0.002	0.999	3.4
Coffee400	0.017	1.67	0.923	347	4.25	0.012	0.995	6.8
Coffee800	0.041	4.27	0.860	318	2.62	0.007	0.957	3
Coffee400Mg	0.021	2.03	0.956	249	3.04	0.021	0.991	11
Coffee800Mg	0.032	5.20	0.864	308	7.08	0.001	0.913	34
NH_3 -N								
EGS400	0.046	36.41	0.951	5.8	37.74	0.001	0.973	11
EGS800	0.053	32.83	0.937	1.8	37.74	0.001	0.987	12
EGS400Mg	0.041	13.32	0.999	26	15.68	0.004	0.998	15
EGS800Mg	0.025	13.91	0.978	61	19.92	0.001	0.957	12
RH400	0.035	42.39	0.987	7.5	19.23	0.001	0.987	13
RH800	0.035	47.21	0.964	4.5	40.32	0.001	0.971	3.4
RH400Mg	0.030	13.91	0.836	136	21.19	0.002	0.980	2.1
RH800Mg	0.098	11.14	0.971	37	10.00	0.012	0.993	6.3
Coffee400	0.036	29.91	0.967	9.7	47.39	0.001	0.757	1.9
Coffee800	0.035	36.80	0.879	96	40.32	0.001	0.971	2.21
Coffee400Mg	0.033	12.10	0.984	19	21.19	0.002	0.980	9.1
Coffee800Mg	0.019	14.74	0.858	49	10.00	0.012	0.993	3.2

The pseudo second-order constant of nitrates was generally higher at 800 °C pyrolysis temperature compared to 400 °C for all unmodified materials. The modification of EGS at 400 and 800 °C resulted in 4 and 2.5 times higher k_{2p} values compared to the modified EGS, respectively. Although the modification of RH and coffee increased the k_{2p} values at 400 °C, compared to the unmodified biochars, modification at 800 °C resulted in lower k_{2p} values. The higher k_{2p} values were observed with the RH400Mg (0.026 g/mg·h) and lower for Coffee800Mg (0.001 g/mg·h). The k_{2p} values of nitrate sorption ranged from 0.02 to 0.022 g/mg·h using hydrogel rice husk biochar composites [47].

Concerning ammonia kinetics, the increase in the pyrolysis temperature did not affect the k_{2p} values of the unmodified materials. The modification of the EGS improved the

k_{2p} value four times only at 400 °C, while the modification of RH and coffee at 400 °C was increased by two times. The k_{2p} values of ammonia were generally lower compared with the other two nutrients. The increase in the pyrolysis temperature from 400 to 800 °C of the modified RH and coffee, resulted in values up to six times higher. Modification enhanced the k_{2p} values up to 12 times for the RH800Mg and Coffee800Mg, compared to the unmodified biochar at 800 °C.

The pseudo-first-order model can be related to physical sorption and the pseudo second-order model assumes that the removal process is controlled by the chemical sorption, which involves the valence forces where the adsorbent and the adsorbate exchange or share electrons [12]. The pseudo second-order model has been reported to better simulate phosphates sorption for biochar from a rice straw/eggshell mixture [12], straw [6], and *rosmarinus officinalis* [7] pyrolyzed at different temperatures.

The diffusion of nutrients by the Weber-Morris model is shown in Figure 4. If the plot of q with $t^{1/2}$ provides a straight line, an intra particle diffusion is involved in the sorption rate and, if the straight line cross the origin, intraparticle diffusion is the rate limiting step [17]. In most cases, two or three linear parts were observed, which implies that different mechanisms are involved in the sorption process. Only Coffee400Mg had one linear segment that passes through the origin. In the case of phosphates, the intercept C in the first linear part was zero for all materials tested, indicating that intra-particle diffusion was the rate-controlling step. The same behavior was also observed with ammonia nitrogen and the majority of nitrate cases, while in the case of EGS800 it was $C = 1.22$ mg/g. Comparing the diffusion constants of the Weber–Morris model (k_{id}), it is shown that in many of the studied cases it was $k_{id1} > k_{id2} > k_{id3}$. The diffusion of molecules in the majority of the sorbents is the determining step of the sorption process, which is also confirmed by the decrease in the k_{id3} value [48]. In the case of phosphates, the k_{id} values were $k_{id1} > k_{id2} > k_{id3}$, except from the RH400 where $k_{id2} < k_{id3}$. A gradual decrease in k_{id} values was also observed with nitrates but not for all the cases. The k_{id} values for EGS800Mg were $k_{id1} > k_{id2}$ and $k_{id2} < k_{id3}$, with the EGS800 constant as $k_{id1} < k_{id2}$. The RH400, RH800, and Coffee800Mg biochars had $k_{id1} = 0$ and thereafter $k_{id2} > k_{id3}$. The RH800 with ammonia nutrients also had $k_{id1} = 0$. Finally, with EGS400 and Coffee400, $k_{id1} > k_{id2}$ and $k_{id2} < k_{id3}$.

The external surface adsorption or instantaneous adsorption occurs in the first step; the second step is the gradual adsorption step, where the intraparticle diffusion is controlled. The third step is the final equilibrium step, where the solute moves slowly from the larger pores to micropores causing a slow adsorption rate. The time required for the second step usually depends on the variations of the system (including solute concentration, temperature, and adsorbent particle size), which is difficult to predict or control [49].

The diffusion of materials depends on the surface's characteristics and the nutrient. The increase in pyrolysis temperature did not considerably affect the number of stages. On the contrary, modification increased the segments of EGS from two to three, remained the same with coffee and decreased the stages from three to two of RH for all examined nutrients.

To estimate the actual rate-limiting step involved in the sorption process, the experimental data were further analyzed by the Boyd model. If the plot of Bt against time is linear and passes through the origin, the intraparticle diffusion controls the rate of mass transfer, while if the plot is nonlinear or linear but does not pass through the origin, the film diffusion or chemical reaction control the sorption rate [17,50]. The Boyd plot shows multi-linearity over the time period studied (Figure 5), without passing through the origin for the majority of the materials examined, thus rendering it quite difficult to predict whether external mass transfer or intra-particle diffusion is the rate controlling step. Only EGS800Mg presented a linear plot and passed through the origin for phosphates and ammonia.

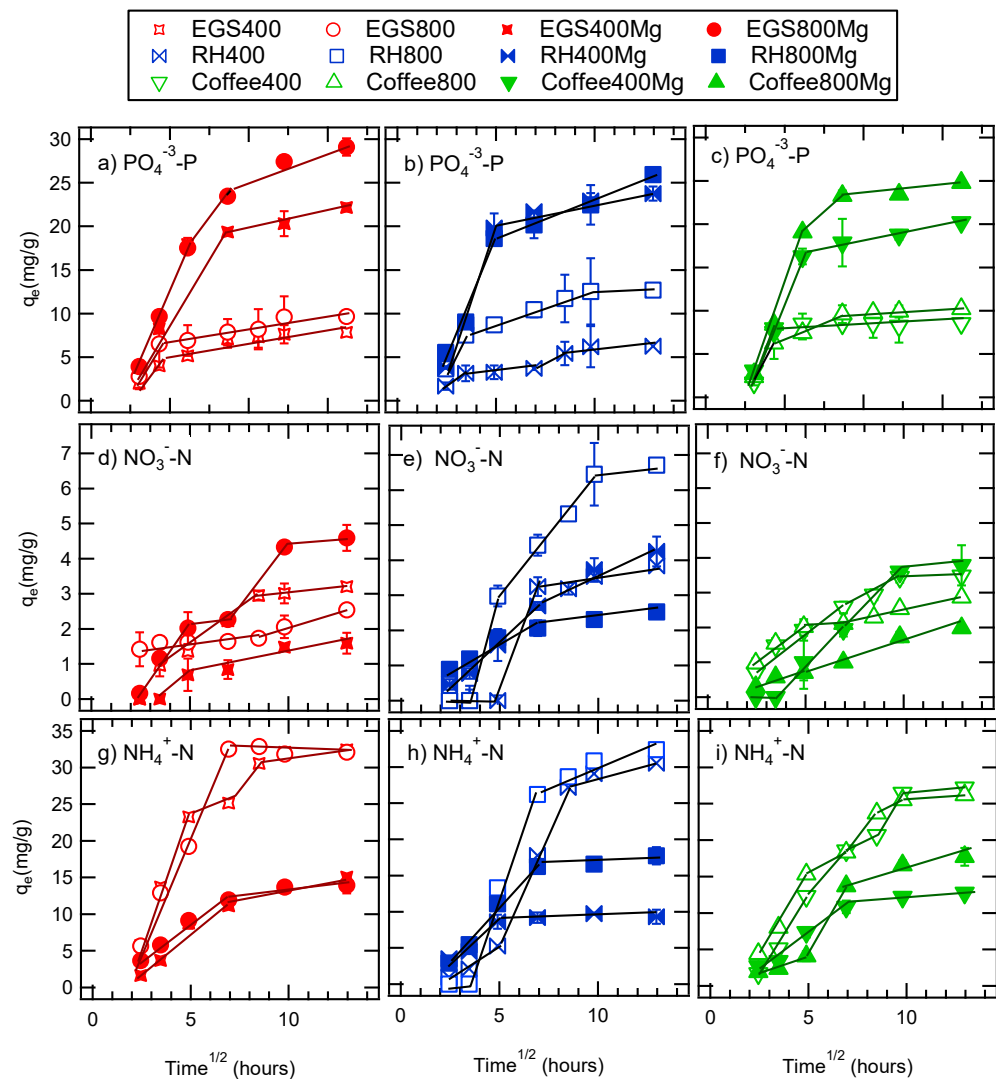


Figure 4. Intraparticle diffusion of: phosphates at an initial concentration of 10 mg $\text{PO}_4^{3-}\text{-P/L}$ for (a) EGS, (b) RH, and (c) Coffee; nitrates at an initial concentration of 2.26 mg $\text{NO}_3\text{-N/L}$ for (d) EGS, (e) RH, and (f) Coffee and ammonia at an initial concentration of 7.77 mg $\text{NH}_3\text{-N/L}$ for (g) EGS, (h) RH, and (i) Coffee.

The pyrolysis temperature seems to affect the sorption capacity of the modified materials for phosphates and nitrates. Generally, biochars pyrolyzed at 800 °C had higher sorption capacity compared to biochars pyrolyzed at 400 °C [51] for the sorption of cadmium with orange peel biochar. The materials pyrolyzed at different temperatures tend to have different morphology and pore structures [16,52]. Modification led to higher sorption capacities for the phosphates of all materials, but the unmodified materials were most efficient to decrease the ammonia concentrations. The modified materials had higher pzc as well, which can increase the sorption capacity of phosphorous due to high pH [29]. Biochars modified by metals have a significantly higher capacity to remove ammonia, nitrates, and phosphates than unmodified biochar, due to the change in the surface charge and the increase in metal oxides on the biochar surface [53]. The modified eggshells at 800 °C had a higher sorption capacity for phosphates and nitrates, but the EGS800 was superior for ammonia. The RH biochar presented a better efficiency in removing phosphates and nitrates compared to EGS. However, nitrate removal was not affected by the modification but only by the temperature.

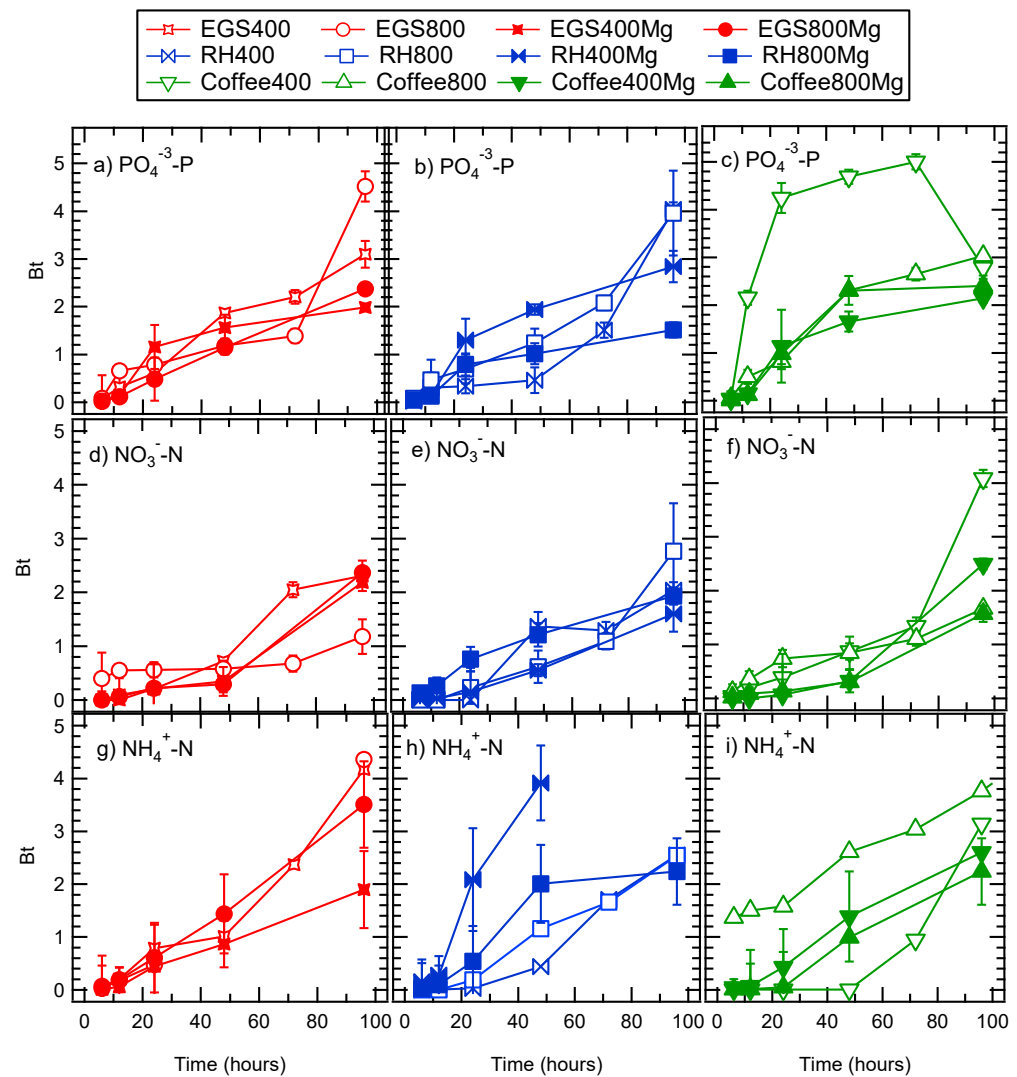


Figure 5. Simulation of Boyd model of: phosphates at an initial concentration of $10 \text{ mg PO}_4^{-3}\text{-P/L}$ for (a) EGS, (b) RH, and (c) Coffee; nitrates at an initial concentration of $2.26 \text{ mg NO}_3\text{-N/L}$ for (d) EGS, (e) RH, and (f) Coffee; and ammonia at an initial concentration of $7.77 \text{ mg NH}_3\text{-N/L}$ for (g) EGS, (h) RH, and (i) Coffee.

3.3. Sorption Isotherm

The isotherm experiments were conducted with biochars exhibiting higher adsorption efficiencies, based on the kinetic experiments results. More specifically, EGS800, EGS800Mg, RH800, and RH800Mg were examined for a period of 48 h and at different nutrient concentrations. The experimental data were fitted with three isotherm models: linear (Figure 6a–c), Langmuir (Figure 6d–f), and Freundlich (Figure 6g–i). The fitting of the experimental results for the three nutrients tested are presented in Table 4. The linear model does not fit the data well. The Langmuir model fits the data better than the Freundlich model. The correlation coefficient (R^2) of the Langmuir isotherm was greater than 0.924 for all materials and nutrients tested, indicating that sorption mainly occurred on the homogeneous surface of biochars [6].

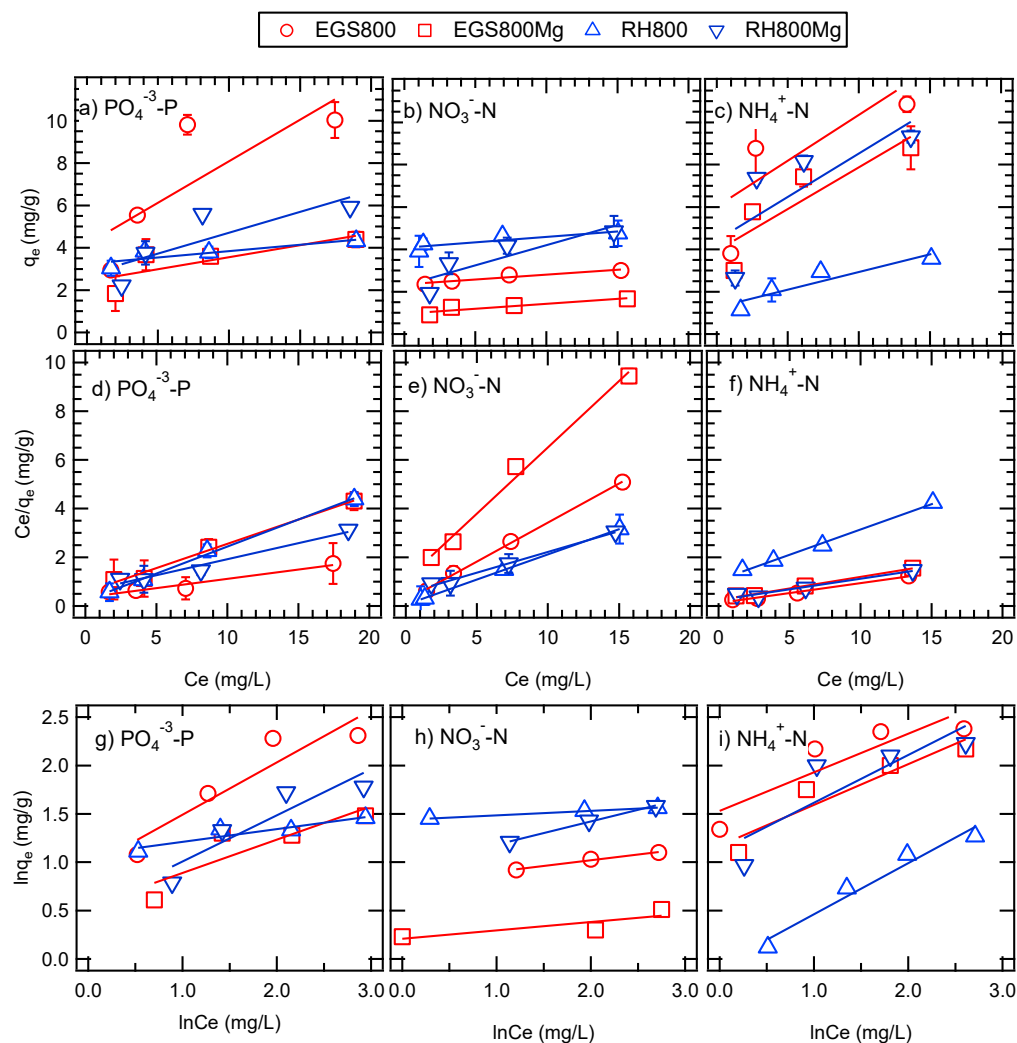


Figure 6. Nutrient uptake by the four materials tested at initial concentration from 2.5 to 20 mg $\text{PO}_4^{3-}\text{-P/L}$, from 2 to 16 mg $\text{NO}_3\text{-N/L}$, and from 2 to 16 mg $\text{NH}_3\text{-N/L}$, solid to liquid ratio of 0.25 g/L and contact time 48 h: (a–c) experimental data, (d–f) linearized form of the Langmuir model equation, and (g–i) linearized form of the Freundlich model equation.

The highest sorption capacity (q_{\max}) for phosphates and ammonium was observed with the EGS800 and was 11.45 mg $\text{PO}_4^{3-}\text{-P/g}$ and 11.59 mg $\text{NH}_3\text{-N/g}$, while the highest nitrates sorption capacity was observed with the RH800Mg (5.24 mg $\text{NO}_3\text{-N}$). Unmodified EGS biochar was more efficient for phosphate and ammonium nutrient. The modified EGS biochars had almost half the sorption capacity for phosphates and nitrates compared to the unmodified materials. Unmodified RH had almost the same sorption capacity (q_{\max}) of 4.37, 4.79, and 4.01 mg/g for phosphates, nitrates, and ammonia, respectively. The modification of RH resulted in higher sorption capacity by 34 and 158% for phosphates and ammonium, respectively, while the differences were not so intense for the nitrates. A comparison of the maximum sorption capacity of the various biochars, reported in the literature, is presented in Table S1. Concerning phosphates, it seems that co-pyrolysis of eggshells and rice straw resulted in notably higher sorption capacities compared to the pristine biochars [12]. The rice straw pyrolyzed at 800 °C yielded a q_{\max} of 5.58 mg phosphates-P/g, but when the eggshells were mixed with rice straw at a mass ratio of 1:1, the produced biochar reached a maximum sorption capacity of 231 mg phosphates-P/g [12]. The peanut shells modified by magnesium and pyrolyzed at 600 °C were most effective since they reached a maximum sorption capacity 94 mg nitrates-N/g [28].

Table 4. Estimated parameters for the isotherm models employed.

Material	Isotherm Model										
	Linear			Langmuir				Freundlich			
	K_H	R^2	RSS	q_{max}	K_L	R^2	RSS	K_F	N	R^2	RSS
(L/g)			(mg/g)	(L/mg)			(mg/g)(L/mg) ^N				
$PO_4^{-3}-P$											
EGS800	0.73	0.465	13	11.45	0.41	0.927	6.9	1.21	0.78	0.850	2.8
EGS800Mg	0.29	0.206	16	4.63	0.66	0.974	62	1.10	0.49	0.850	1.1
RH800	0.3	0.365	16	4.37	1.73	0.995	52	1.23	0.40	0.632	0.22
RH800Mg	0.41	0.438	15	6.62	0.43	0.941	33	1.09	0.43	0.908	0.01
$NO_3^{-}-N$											
EGS800	0.26	0.39	12	3.04	2.48	0.998	7.6	1.19	0.31	0.604	2.3
EGS800Mg	0.13	0.148	13	1.71	0.93	0.983	3.5	0.96	0.21	0.857	1.9
RH800	0.41	0.96	10	4.79	6.63	1	1.8	1.47	0.29	0.292	0.23
RH800Mg	0.41	0.427	11	5.24	0.63	0.965	3.2	1.47	0.29	0.877	0.3
NH_3-N											
EGS800	1.06	0.164	7	11.59	1.14	0.982	1.8	1.47	0.72	0.634	8.0
EGS800Mg	0.79	0.413	9	9.54	0.69	0.97	4.9	1.32	0.69	0.737	2.6
RH800	0.28	0.669	12	4.01	0.4	0.929	82	0.99	0.51	0.974	4.9
RH800Mg	0.86	0.355	8.5	10.34	0.62	0.941	4.4	0.99	0.51	0.753	3.5

From the presented results it can be summarized that the presence of Mg^{2+} and Ca^{2+} is favorable for the adsorption of phosphates, as can be seen in Figure 3. The SSA values are not a decisive factor for adsorption. It probably denotes that the reaction between Mg^{2+} (and Ca^{2+} for the eggshell samples) with phosphates is responsible for the higher values of adsorption. On the other hand, the presence of Mg^{2+} and Ca^{2+} has a detrimental effect on the adsorption of NH_3-N . Indeed, in this case, the modification process is not working well. The differences in the sorption capacity between the biochars pyrolyzed at 400 °C and 800 °C are rather small, if any, although the differences in the SSA values are high, especially for the coffee and RH samples. Interestingly, the pzc of the samples seems to influence the adsorption capacity. The samples with higher basicity and higher values of pzc result in higher sorption. Thermodynamic studies have shown that the sorption of phosphates [54] and ammonia nitrogen [55] is an endothermic reaction and that the maximum sorption is achieved at higher temperatures.

The $NO_3^{-}-N$ adsorption is more complicated. There is not a clear trend with either the SSA, Mg^{2+} content, or pzc value. This can be partially attributed to the low values of sorption efficiency determined suggesting that the presence of Mg^{2+} and the surface basicity are not the decisive parameters for the sorption process. For the RH and coffee samples, the modification with Mg and high pyrolysis temperature result in lower adsorption of nitrates, while the modification of the samples pyrolyzed at 400 °C do not change the sorption efficiency. The picture is quite different for the EGS samples, where the modification has a positive effect for the 800 °C and a negative for the 400 °C cases.

One possible explanation is that the sorption process can be influenced from the surface groups, which do not participate in the phosphates or the NH_3-N sorption. These groups generally consist of carbon species with different speciation and oxidation states and surface O-containing species and they are active for surface reactions [56]. The surface groups increase with the pyrolysis temperature and without modification. On the other hand, modification with Mg and high pyrolysis temperatures consumed these sites and disturbed the sorption. This is valid for the RH and coffee samples. In the case of the EGS samples, the presence of Mg^{2+} is limited and the modification with high pyrolysis temperatures improved the sorption capacity.

4. Conclusions

A comparative study of different food waste processing materials such as eggshells, rice husks, and spent coffee grains was conducted for the removal of phosphates, nitrates, and ammonia from water. The materials were pyrolyzed at 400 and 800 °C with and without magnesium modification. The kinetic experiments demonstrated that the magnesium-modified EGS pyrolyzed at 800 °C were superior for the removal of phosphates (27.3 mg P/g), while the RH pyrolyzed at 800 °C performed better for the removal of nitrates and ammonia nitrogen, yielding sorption efficiency of 6.8 and 33.2 mg N/mg, respectively. The modification of biochars resulted in better sorption capacities for phosphates for the three materials tested. On the contrary, biochar modification did not favor the removal of nitrates and ammonia nitrogen. In the case of ammonia, raw biochars exhibited better performance. The pzc of the biochars seems to affect the sorption capacity. The samples with higher basicity and higher values of pzc result in higher sorption efficiencies. The materials investigated are easily available from local enterprises and local shops and their use contributes to the valorization of food wastes and the minimization of waste quantities disposed. Additional research work is needed to investigate the performance of biochars in removing nutrients using real water and wastewater and the scaling up of the sorption processes.

Supplementary Materials: The following supporting information can be downloaded at: <https://www.mdpi.com/article/10.3390/su142416483/s1>, Figure S1: Materials examined, Table S1: Sorption capacity of various biochars for phosphates, nitrates, and ammonia; Table S2: Scanning electron microscope images of the biochars studied.

Author Contributions: S.E.B.: Investigation, Formal Analysis, and Writing. J.V.: Investigation and Writing—review and editing. I.D.M.: Conceptualization, Funding acquisition, and Editing. All authors have read and agreed to the published version of the manuscript.

Funding: S.E. Biliani and I.D. Manariotis acknowledge support of this work, which was created as part of the project “BLUE-GREENWAY: Innovative solutions for improving the environmental status of eutrophic and anoxic coastal ecosystems”, funded by Iceland, Liechtenstein, and Norway through the EEA and Norway Grants Fund for Regional Cooperation (2018-1-0284).

Institutional Review Board Statement: Not applicable.

Informed Consent Statement: Not applicable.

Data Availability Statement: Not applicable.

Conflicts of Interest: The authors declare no conflict of interest.

References

1. Sirajo, L.; Zaini, M.A.A. Existing and Emerging Technologies for the Removal of Orthophosphate from Wastewater by Agricultural Waste Adsorbents: A Review. *Biomass. Convers. Biorefinery* **2022**, 1–17. [CrossRef]
2. Zamparas, M.; Zacharias, I. Restoration of Eutrophic Freshwater by Managing Internal Nutrient Loads. A Review. *Sci. Total Environ.* **2014**, *496*, 551–562. [CrossRef] [PubMed]
3. Xiang, W.; Zhang, X.; Chen, J.; Zou, W.; He, F.; Hu, X.; Tsang, D.C.W.; Ok, Y.S.; Gao, B. Biochar Technology in Wastewater Treatment: A Critical Review. *Chemosphere* **2020**, *252*, 126539. [CrossRef]
4. Tang, M.; Deng, Q.; Li, X.; Cao, X.; Zhang, Z.; Zhou, Y.; Sun, Q.; Song, C. The Effect of Natural Materials Used as Sediment Remediation on Phosphorus and Nitrogen Control in a Mesocosm. *Environ. Sci. Eur.* **2020**, *32*, 90. [CrossRef]
5. Reddy, K.R.; Xie, T.; Dastgheibi, S. Nutrients Removal from Urban Stormwater by Different Filter Materials. *Water Air Soil Pollut.* **2014**, *225*, 1778. [CrossRef]
6. Miao, Q.; Li, G. Potassium Phosphate/Magnesium Oxide Modified Biochars: Interfacial Chemical Behaviours and Pb Binding Performance. *Sci. Total Environ.* **2021**, *759*, 143452. [CrossRef] [PubMed]
7. Mohammadi, R.; Hezarjaribi, M.; Ramasamy, D.L.; Sillanpää, M.; Pihlajamäki, A. Application of a Novel Biochar Adsorbent and Membrane to the Selective Separation of Phosphate from Phosphate-Rich Wastewaters. *Chem. Eng. J.* **2021**, *407*, 126494. [CrossRef]
8. Mrozik, W.; Rajaeifar, M.A.; Heidrich, O.; Christensen, P. Environmental Impacts, Pollution Sources and Pathways of Spent Lithium-Ion Batteries. *Energy Environ. Sci.* **2021**, *14*, 6099–6121. [CrossRef]

9. Yaashikaa, P.R.; Kumar, P.S.; Varjani, S.; Saravanan, A. A Critical Review on the Biochar Production Techniques, Characterization, Stability and Applications for Circular Bioeconomy. *Biotechnol. Rep.* **2020**, *28*, e00570. [[CrossRef](#)]
10. Pang, S. Advances in Thermochemical Conversion of Woody Biomass to Energy, Fuels and Chemicals. *Biotechnol. Adv.* **2019**, *37*, 589–597. [[CrossRef](#)] [[PubMed](#)]
11. Lin, Y.; Ma, X.; Peng, X.; Yu, Z.; Fang, S.; Lin, Y.; Fan, Y. Combustion, Pyrolysis and Char CO₂-Gasification Characteristics of Hydrothermal Carbonization Solid Fuel from Municipal Solid Wastes. *Fuel* **2016**, *181*, 905–915. [[CrossRef](#)]
12. Liu, X.; Shen, F.; Qi, X. Adsorption Recovery of Phosphate from Aqueous Solution by CaO-Biochar Composites Prepared from Eggshell and Rice Straw. *Sci. Total Environ.* **2019**, *666*, 694–702. [[CrossRef](#)] [[PubMed](#)]
13. Peng, Y.; Sun, Y.; Fan, B.; Zhang, S.; Bolan, N.S.; Chen, Q.; Tsang, D.C.W. Fe/Al (Hydr)Oxides Engineered Biochar for Reducing Phosphorus Leaching from a Fertile Calcareous Soil. *J. Clean. Prod.* **2021**, *279*, 123877. [[CrossRef](#)]
14. Roy, A.; Chaturvedi, S.; Singh, S.V.; Kasivelu, G.; Dhyani, V.C.; Pyne, S. Preparation and Evaluation of Two Enriched Biochar-Based Fertilizers for Nutrient Release Kinetics and Agronomic Effectiveness in Direct-Seeded Rice. *Biomass Convers. Biorefinery* **2022**, 1–12. [[CrossRef](#)]
15. Das, S.K.; Ghosh, G.K.; Choudhury, B.U.; Hazarika, S.; Mishra, V.K. Developing Biochar and Organic Nutrient Packages/Technology as Soil Policy for Enhancing Yield and Nutrient Uptake in Maize-Black Gram Cropping System to Maintain Soil Health. *Biomass Convers. Biorefinery* **2022**, 1–13. [[CrossRef](#)]
16. Das, S.K.; Ghosh, G.K.; Avasthe, R. Valorizing Biomass to Engineered Biochar and Its Impact on Soil, Plant, Water, and Microbial Dynamics: A Review. *Biomass Convers. Biorefinery* **2020**, *12*, 4183–4199. [[CrossRef](#)]
17. Orfanos, A.G.; Manariotis, I.D.; Karapanagioti, H.K. Removal of Methylene Blue from Water by Food Industry By-Products and Biochars. *Desalin. Water Treat.* **2018**, *103*, 113–121. [[CrossRef](#)]
18. Lykoudi, A.; Frontistis, Z.; Vakros, J.; Manariotis, I.D.; Mantzavinos, D. Degradation of Sulfamethoxazole with Persulfate Using Spent Coffee Grounds Biochar as Activator. *J. Environ. Manag.* **2020**, *271*, 111022. [[CrossRef](#)] [[PubMed](#)]
19. Tombarkiewicz, B.; Antonkiewicz, J.; Lis, M.W.; Pawlak, K.; Trela, M.; Witkiewicz, R.; Gorczyca, O. Chemical Properties of the Coffee Grounds and Poultry Eggshells Mixture in Terms of Soil Improver. *Sci. Rep.* **2022**, *12*, 2592. [[CrossRef](#)] [[PubMed](#)]
20. Avramiotis, E.; Frontistis, Z.; Manariotis, I.D.; Vakros, J.; Mantzavinos, D. Oxidation of Sulfamethoxazole by Rice Husk Biochar-Activated Persulfate. *Catalysts* **2021**, *11*, 850. [[CrossRef](#)]
21. Mirmohamadsadeghi, S.; Karimi, K. Recovery of Silica from Rice Straw and Husk. In *Current Developments in Biotechnology and Bioengineering*; Elsevier: Amsterdam, The Netherlands, 2020; pp. 481–490. ISBN 978-0-444-64321-6.
22. Avramiotis, E.; Frontistis, Z.; Manariotis, I.D.; Vakros, J.; Mantzavinos, D. On the Performance of a Sustainable Rice Husk Biochar for the Activation of Persulfate and the Degradation of Antibiotics. *Catalysts* **2021**, *11*, 1303. [[CrossRef](#)]
23. Waheed, M.; Yousaf, M.; Shehzad, A.; Inam-Ur-Raheem, M.; Khan, M.K.I.; Khan, M.R.; Ahmad, N.; Abdullah, R.M.A. Channelling Eggshell Waste to Valuable and Utilizable Products: A Comprehensive Review. *Trends Food Sci. Technol.* **2020**, *106*, 78–90. [[CrossRef](#)]
24. Ajala, E.; Eletta, O.A.A.; Ajala, M.A.; Oyenyi, K. Characterization and Evaluation of Chicken Eggshell for Use as a Bio-Resource. *Chem. Environ. Eng.* **2018**, *14*, 26–40.
25. Liu, H.; Liu, Y.; Tang, L.; Wang, J.; Yu, J.; Zhang, H.; Yu, M.; Zou, J.; Xie, Q. Egg Shell Biochar-Based Green Catalysts for the Removal of Organic Pollutants by Activating Persulfate. *Sci. Total Environ.* **2020**, *745*, 141095. [[CrossRef](#)] [[PubMed](#)]
26. Panagiotou, E.; Kafa, N.; Koutsokeras, L.; Kouis, P.; Nikolaou, P.; Constantinides, G.; Vyrides, I. Turning Calcined Waste Egg Shells and Wastewater to Brushite: Phosphorus Adsorption from Aqua Media and Anaerobic Sludge Leach Water. *J. Clean. Prod.* **2018**, *178*, 419–428. [[CrossRef](#)]
27. Yirong, C.; Vaurs, L.P. Wasted Salted Duck Eggshells as an Alternative Adsorbent for Phosphorus Removal. *J. Environ. Chem. Eng.* **2019**, *7*, 103443. [[CrossRef](#)]
28. Zhang, M.; Gao, B.; Yao, Y.; Xue, Y.; Inyang, M. Synthesis of Porous MgO-Biochar Nanocomposites for Removal of Phosphate and Nitrate from Aqueous Solutions. *Chem. Eng. J.* **2012**, *210*, 26–32. [[CrossRef](#)]
29. Yang, F.; Chen, Y.; Nan, H.; Pei, L.; Huang, Y.; Cao, X.; Xu, X.; Zhao, L. Metal Chloride-Loaded Biochar for Phosphorus Recovery: Noteworthy Roles of Inherent Minerals in Precursor. *Chemosphere* **2021**, *266*, 128991. [[CrossRef](#)]
30. Takaya, C.A.; Fletcher, L.A.; Singh, S.; Okwuosa, U.C.; Ross, A.B. Recovery of Phosphate with Chemically Modified Biochars. *J. Environ. Chem. Eng.* **2016**, *4*, 1156–1165. [[CrossRef](#)]
31. Thant Zin, M.M.; Kim, D.J. Simultaneous Recovery of Phosphorus and Nitrogen from Sewage Sludge Ash and Food Wastewater as Struvite by Mg-Biochar. *J. Hazard. Mater.* **2021**, *403*, 123704. [[CrossRef](#)]
32. Weber, W.; Morris, J.C. Kinetics of Adsorption on Carbon from Solution. *J. Sanit. Eng. Div. Am. Soc. Civ. Eng.* **1963**, *89*, 31–60. [[CrossRef](#)]
33. Boyd, G.E.; Schubert, J.; Adamson, A.W. The Exchange Adsorption of Ions from Aqueous Solutions by Organic Zeolites. Ion-Exchange Equilibria. *J. Am. Chem. Soc.* **1947**, *69*, 2818–2829. [[CrossRef](#)] [[PubMed](#)]
34. Reichenberg, D. Properties of Ion-Exchange Resins in Relation to Their Structure. Part I. Titration Curves. *J. Chem. Soc.* **1952**, 2836, 3299–3303. [[CrossRef](#)]
35. Tsavatopoulou, V.D.; Manariotis, I.D. The Effect of Surface Properties on the Formation of *Scenedesmus Rubescens* Biofilm. *Algal Res.* **2020**, *52*, 102095. [[CrossRef](#)]

36. APHA; WEF; AWWA. *Standard Methods for the Examination of Water and Wastewater*, 20th ed.; Clesceri, L.S., Greenberg, A.E., Eaton, A.D.A., Eds.; American Public Health Association, American Water Works Association, Water Environment Federation: Washington, DC, USA, 2012.
37. Fresenius, W.; Quentin, K.E.; Schneider, W.; Bibo, F.-J.; Birke, H.; Böhm, H.; Czysz, W.; Gorbauch, H.; Hoffmann, H.J.; Rump, H.-H.; et al. *Water Analysis; a Practical Guide to Physico-Chemical, Chemical and Microbiological Water Examination and Quality Assurance*; Fresenius, W., Quentin, K.E., Schneider, W., Eds.; Deutsche Gesellschaft für Technische Zusammenarbeit: Bonn, Germany, 1988; ISBN 9788578110796.
38. Akhtar, L.; Ahmad, M.; Iqbal, S.; Abdelhafez, A.A.; Mehran, M.T. Biochars' Adsorption Performance towards Moxifloxacin and Ofloxacin in Aqueous Solution: Role of Pyrolysis Temperature and Biomass Type. *Environ. Technol. Innov.* **2021**, *24*, 101912. [[CrossRef](#)]
39. Albalasmeh, A.; Gharaibeh, M.A.; Mohawesh, O.; Alajlouni, M.; Quzaih, M.; Masad, M.; El Hanandeh, A. Characterization and Artificial Neural Networks Modelling of Methylene Blue Adsorption of Biochar Derived from Agricultural Residues: Effect of Biomass Type, Pyrolysis Temperature, Particle Size. *J. Saudi Chem. Soc.* **2020**, *24*, 811–823. [[CrossRef](#)]
40. Manariotis, I.D.; Fotopoulou, K.N.; Karapanagioti, H.K. Preparation and Characterization of Biochar Sorbents Produced from Malt Spent Rootlets. *Ind. Eng. Chem. Res.* **2015**, *54*, 9577–9584. [[CrossRef](#)]
41. Stanienda-Pilecki, K.J. The Importance of Fourier-Transform Infrared Spectroscopy in the Identification of Carbonate Phases Differentiated in Magnesium Content. *Spectroscopy* **2019**, *34*, 32–42.
42. Qian, L.; Guo, F.; Jia, X.; Zhan, Y.; Zhou, H.; Jiang, X.; Tao, C. Recent Development in the Synthesis of Agricultural and Forestry Biomass-Derived Porous Carbons for Supercapacitor Applications: A Review. *Ionics* **2020**, *26*, 3705–3723. [[CrossRef](#)]
43. Andrade, T.S.; Vakros, J.; Mantzavinos, D.; Lianos, P. Biochar Obtained by Carbonization of Spent Coffee Grounds and Its Application in the Construction of an Energy Storage Device. *Chem. Eng. J. Adv.* **2020**, *4*, 100061. [[CrossRef](#)]
44. Zhang, B.; Lens, P.N.L.; Shi, W.; Zhang, R.; Zhang, Z.; Guo, Y.; Bao, X.; Cui, F. Enhancement of Aerobic Granulation and Nutrient Removal by an Algal–Bacterial Consortium in a Lab-Scale Photobioreactor. *Chem. Eng. J.* **2018**, *334*, 2373–2382. [[CrossRef](#)]
45. Cui, X.; Lu, M.; Khan, M.B.; Lai, C.; Yang, X.; He, Z.; Chen, G.; Yan, B. Hydrothermal Carbonization of Different Wetland Biomass Wastes: Phosphorus Reclamation and Hydrochar Production. *Waste Manag.* **2020**, *102*, 106–113. [[CrossRef](#)] [[PubMed](#)]
46. Liu, Y.; Lou, X. Removal of Phosphorus Using Biochar Derived from Fenton Sludge: Mechanism and Performance Insights. *Water Environ. Res.* **2022**, *94*, e10763. [[CrossRef](#)]
47. Sadeghi Afjeh, M.; Bagheri Marandi, G.; Zohuriaan-Mehr, M.J. Nitrate Removal from Aqueous Solutions by Adsorption onto Hydrogel-Rice Husk Biochar Composite. *Water Environ. Res.* **2020**, *92*, 934–947. [[CrossRef](#)]
48. Campos, N.; Barbosa, C.; Rodriguez-Diaz, J.; Duarte, M. Removal of Naphthenic Acids Using Activated Charcoal: Kinetic and Equilibrium Studies. *Adsorpt. Sci. Technol.* **2018**, *36*, 1405–1421. [[CrossRef](#)]
49. Wu, F.C.; Tseng, R.L.; Juang, R.S. Initial Behavior of Intraparticle Diffusion Model Used in the Description of Adsorption Kinetics. *Chem. Eng. J.* **2009**, *153*, 1–8. [[CrossRef](#)]
50. Labanya, R.; Srivastava, P.C.; Pachauri, S.P.; Shukla, A.K.; Shrivastava, M.; Srivastava, P. Kinetics of Micronutrients and S Adsorption onto Phyto-Biochars: Influence of Pyrolysis Temperatures and Properties of Phyto-Biochars. *Biomass Convers. Biorefinery* **2022**, 1–15. [[CrossRef](#)]
51. Tran, H.N.; You, S.J.; Chao, H.P. Effect of Pyrolysis Temperatures and Times on the Adsorption of Cadmium onto Orange Peel Derived Biochar. *Waste Manag. Res.* **2016**, *34*, 129–138. [[CrossRef](#)]
52. Wang, B.; Ma, Y.; Lee, X.; Wu, P.; Liu, F.; Zhang, X.; Li, L.; Chen, M. Environmental-Friendly Coal Gangue-Biochar Composites Reclaiming Phosphate from Water as a Slow-Release Fertilizer. *Sci. Total Environ.* **2021**, *758*, 143664. [[CrossRef](#)]
53. Zhang, M.; Song, G.; Gelardi, D.L.; Huang, L.; Khan, E.; Mašek, O.; Parikh, S.J.; Ok, Y.S. Evaluating Biochar and Its Modifications for the Removal of Ammonium, Nitrate, and Phosphate in Water. *Water Res.* **2020**, *186*, 3321–3328. [[CrossRef](#)]
54. Karunanithi, R.; Ok, Y.S.; Dharmarajan, R.; Ahmad, M.; Seshadri, B.; Bolan, N.; Naidu, R. Sorption, Kinetics and Thermodynamics of Phosphate Sorption onto Soybean Stover Derived Biochar. *Environ. Technol. Innov.* **2017**, *8*, 113–125. [[CrossRef](#)]
55. Xue, S.; Zhang, X.; Ngo, H.H.; Guo, W.; Wen, H.; Li, C.; Zhang, Y.; Ma, C. Food Waste Based Biochars for Ammonia Nitrogen Removal from Aqueous Solutions. *Bioresour. Technol.* **2019**, *292*, 121927. [[CrossRef](#)] [[PubMed](#)]
56. Ntzoufra, P.; Vakros, J.; Frontistis, Z.; Tsatsos, S.; Kyriakou, G.; Kennou, S.; Manariotis, I.D.; Mantzavinos, D. Effect of Sodium Persulfate Treatment on the Physicochemical Properties and Catalytic Activity of Biochar Prepared from Spent Malt Rootlets. *J. Environ. Chem. Eng.* **2021**, *9*, 105071. [[CrossRef](#)]